Physics of Plasmas

Effect of cross-beam energy transfer on target-offset asymmetry in direct-drive inertial confinement fusion implosions

Cite as: Phys. Plasmas **27**, 112713 (2020); https://doi.org/10.1063/5.0015781
Submitted: 30 May 2020 . Accepted: 23 October 2020 . Published Online: 17 November 2020

K. S. Anderson, C. J. Forrest, O. M. Mannion, F. J. Marshall, R. C. Shah, D. T. Michel, J. A. Marozas, P. B. Radha, D. H. Edgell, R. Epstein, V. N. Goncharov, J. P. Knauer, M. Gatu Johnson, and S. Laffite

Physics of Plasmas ARTICLE scitation.org/journal/php

Effect of cross-beam energy transfer on target-offset asymmetry in direct-drive inertial confinement fusion implosions

Cite as: Phys. Plasmas **27**, 112713 (2020); doi: 10.1063/5.0015781
Submitted: 30 May 2020 · Accepted: 23 October 2020 ·
Published Online: 17 November 2020

K. S. Anderson,[1,a)] C. J. Forrest,[1] O. M. Mannion,[1] F. J. Marshall,[1] R. C. Shah,[1] D. T. Michel,[1,2] J. A. Marozas,[1] P. B. Radha,[1] D. H. Edgell,[1] R. Epstein,[1] V. N. Goncharov,[1] J. P. Knauer,[1] M. Gatu Johnson,[3] and S. Laffite[4]

AFFILIATIONS

[1]University of Rochester, Laboratory for Laser Energetics, Rochester, New York 14623, USA
[2]ONERA/DOTA Université Paris Saclay, F-91123 Palaiseau, France
[3]Plasma Science and Fusion Center, Massachusetts Institute of Technology, Cambridge, Massachusetts 02139, USA
[4]Commissariat à l'Energie Atomique, DAM, DIF, F-91297 Arpajon, France

[a)]**Author to whom correspondence should be addressed:** kand@lle.rochester.edu

ABSTRACT

The unintentional mispositioning of inertial confinement fusion (ICF) capsules from the center of laser beam convergence has long been shown in simulations to generate large $\ell = 1$ asymmetry and significantly degrade implosion symmetry and fusion yields. Experimental yields on the OMEGA laser system, however, have shown much less sensitivity to this initial target offset. This paper presents simulations of offset ICF implosions improved by including a physics model of cross-beam energy transfer (CBET), a mechanism of laser energy scattering from one beam to another. Room-temperature OMEGA implosion experiments with prescribed target offsets are simulated with and without CBET, illustrating that CBET mitigates the $\ell = 1$ implosion asymmetry from the target offset. Comparison of simulations to multiple complementary experimental observables indicates that the addition of CBET physics in offset simulations is necessary to match experimental results.

I. INTRODUCTION

In direct-drive[1] inertial confinement fusion (ICF),[2] multiple laser beams are directed onto a spherical microcapsule filled with a deuterium (D_2) or a deuterium–tritium (DT) fuel mixture. The laser energy is absorbed in the outer layers of the capsule, causing mass ablation, which drives a spherical compression of the capsule by a radial factor of 15 to 35. As the capsule compresses, the fuel in the cold capsule shell is compressed to a high density (>100 g/cm^3), with a central hot spot forming interior to the shell with a high temperature (of the order of a few to 10 keV) suitable for high fusion-reaction rates. As the target implodes, however, nonuniformities in the capsule and laser drive symmetry can cause capsule perturbations, which are amplified by hydrodynamic instabilities.[3–5] These perturbations deform the resulting hot spot, reducing the overall compression and hot-spot temperature, thereby degrading the fusion yield.

It is well known that at typical ICF laser intensities (of the order of 5 to 10×10^{14} W/cm^2), cross-beam energy transfer (CBET)[6–8] can cause significant laser energy losses to directly driven capsules. CBET occurs in a direct-drive plasma when incoming laser light from one beam interacts with refracted, outgoing light from other beams, stealing some energy from the incoming light and scattering that energy away from the target along the path of the outgoing light rays. This effect occurs in the low-density corona formed by the ablating plasma, when the two crossing light waves interact with an ion acoustic wave in the plasma. High-intensity pump and seed intensity as well as long density and velocity scale lengths provide favorable conditions for high CBET scattering. This energy transfer typically occurs well before the incoming light wave reaches the plasma critical surface, where laser light is most efficiently absorbed by the plasma, meaning that light scattered by CBET is typically not absorbed into the plasma. This can result in large energy losses to the system. For example, the absorbed energy loss[9] due to CBET from a 351-nm laser system may be of the order of 10% to 20% at an intensity of 5×10^{14} W/cm^2 with a plasma density scale length about 150 to 200 μm.

CBET losses result in a decrease in the ablation pressure, shell implosion velocity, and compression of the capsule, leading to lower fusion yield. The effects of CBET on the one-dimensional (1D) physics of direct-drive ICF are well documented.[9,10] However, due to the computational expense of including CBET physics in simulations, it has only been in recent years that CBET has been included in multidimensional simulations of direct-drive ICF implosions.[11–13]

Historically, flux limited[14] Spitzer–Härm[15] thermal transport models were used in simulation to account for discrepancies in laser drive efficiency between simulations and experiments. Flux limiters were typically tuned to a single time-independent value to best match the experimental observables. For a certain class of direct-drive ICF implosions (mainly with square-pulse or other simple laser histories), this model was long deemed sufficient to capture the observables of yield and bang time (time of peak neutron production) using flux limiter values of the order of 0.06 to 0.10 (see Refs. 1, p. 90, and 16). However, as ICF designs evolved, it was clear that more complex shaped pulse designs required more sophisticated models to adequately model direct-drive implosions.

When CBET was identified as playing a significant role in direct-drive implosions, models were introduced into a few radiation–hydrodynamic codes to account for this physics effect.[9,11,12] However, the computational run time for the CBET models was significantly higher (four to ten times longer) than for previous flux-limited models. This was, at the time, computationally prohibitive for multi-dimensional simulations. As a result, some designers began using 1D simulations to tune the flux limiter by varying its value in time[17] to match the 1D time-evolution of the implosion from the more detailed, time-consuming simulations including both nonlocal thermal transport (NLTT) and CBET physics. They would then use the same time history for the variable flux limiter (VFL) values in multi-dimensional simulations to decrease run time and improve simulation throughput. The argument for doing so was that as long as the shell and shock trajectories were the same (i.e., same adiabat and shell acceleration), the evolution and effects of the multi-dimensional hydrodynamic instabilities would be similar.

One major source of implosion nonuniformity is target mispositioning or offset. When the target is mispositioned with respect to the center of convergence of the laser beams, a perturbation with a dominant $\ell = 1$ mode is present in the illumination pattern on target,[18–20] with the "hot side" (the side with higher illumination) being opposite to the direction of the offset. This nonuniformity arises because the distance between beam centers on the target surface becomes smaller on the hot side and larger on the cold side. Previous simulations[18–21] of high-performance cryogenic implosions on the 60-beam OMEGA laser system[22] indicate that this $\ell = 1$ perturbation from target offset persists in time at high amplitude, resulting in highly degraded yields and distorted hot spots, even when target offsets are small (40% to 50% yield degradation with 20-μm offset, which is about 4% of the capsule radius for typical OMEGA capsules). Reference 23 also shows that $\ell = 1$ mode perturbations can significantly degrade implosion performance. In contrast, experimental fusion yields from cryogenic implosions on OMEGA have shown relatively low sensitivity to target offsets of this magnitude.[24] This discrepancy between simulations and experiments has not been previously understood.

To study the effect of target offset in a more controlled environment, experiments with room-temperature capsules were performed on OMEGA with prescribed offsets. These room-temperature experiments are simpler to field on OMEGA and require no cryogenic target handling or shroud, allowing more precise control of target positioning. For comparison, target mispositioning in room-temperature implosions on OMEGA is consistently of the order of 5 μm or less, whereas cryogenic target offsets may vary up to 40 μm or more. Furthermore, these capsules have no cryogenic fuel layer, which typically represents a large and variable source of implosion nonuniformity and further complicates analysis. In this text, results from multiple, complementary diagnostics from these room-temperature experiments are presented and compared with simulated observables generated from two-dimensional (2D) *DRACO*[25] simulations and using *SPECT3D*,[26] an x-ray imaging postprocessor, to generate simulated x-ray radiographs. Comparisons between CBET and variable-flux-limiter (VFL) simulations illustrate a mitigating effect of CBET on the $\ell = 1$ laser drive nonuniformity, hot-spot x-ray core asymmetry, and yield degradation.

This paper makes the statement that the VFL model of direct-drive implosions is not appropriate in the case of modeling nonuniformity due to target offset and illustrates the mitigating effect of CBET physics to support this statement. Furthermore, it is concluded that modeling 3D CBET physics in offset simulations is essential to adequately match all of these experimental observables.

II. EXPERIMENTAL SETUP

The targets used in the experiment consisted of a single-layer plastic (CH) capsule with a thickness of 27.0 ± 0.6 μm and an outer radius of 434.6 ± 1.2 μm (see Fig. 1). The capsules were filled with either 20 atm of D_2 or 15 atm of DT (30% D, 70% T) gas. A thin 0.1 μm aluminum overcoat was added after filling to retain the gas fill and prevent leakage. The laser system delivered a total energy of 21.3 ± 0.5 kJ to the target in an adiabat-shaping[27,28] temporal pulse history (see Fig. 1) with a single Gaussian picket of 70-ps full width at

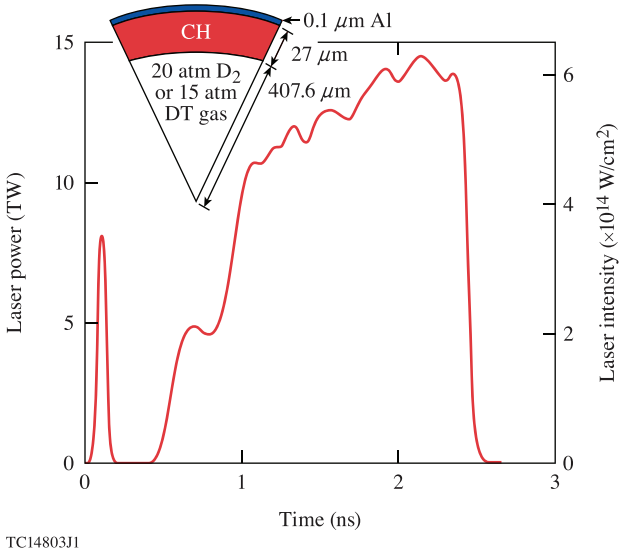

FIG. 1. Laser pulse temporal history in TW and the nominal laser intensity (power divided by initial target surface area or "vacuum hardsphere" intensity) are plotted. The inset shows average capsule parameters for the OMEGA experiments.

half maximum and a total power of 9 TW, a 250-ps foot at 5 TW, and a 12- to 14-TW main drive pulse of 1.5-ns duration. The nominal intensity of the laser pulse, defined as the laser power divided by the target surface area at $t = 0$, is shown by the right-hand vertical axis in Fig. 1 and peaks at approximately 6×10^{14} W/cm^2. The total pulse duration was 2.5 ns and compressed the capsule to a convergence ratio of 15 on an average in-flight shell adiabat (simulated) of 3.7. Here, the convergence ratio is defined as the initial inner target radius divided by the minimum hot-spot radius (defined using the point interior to the shell where the density falls to $1/e$ of the maximum shell density) at the time of peak compression and the average adiabat is defined as the ratio of the shell pressure to the Fermi-degenerate pressure at the same density and is mass averaged over the unablated shell material at the time of peak shell velocity. All OMEGA beams used SG5 phase plates, which result in focal spots at the target plane that are approximately round with super-Gaussian radial profiles having a super-Gaussian exponent of 4.44 and half-width at $1/e$ of the peak intensity of 360 μm.

Four prescribed offsets were shot for each gas fill: the first was at the center of beam convergence or target chamber center (TCC), i.e., no offset; the other three were 40-μm offsets, one toward the P6 location of the OMEGA target chamber, another in the opposite direction toward P7, and the last in an orthogonal direction to the P6–P7 line of sight. For reference, the (θ, ϕ) angular coordinates of the P6, P7 port locations and those of the orthogonal offset direction are approximately (63.4°, 342.0°), (116.6°, 162.0°), and (89.4°, 71.1°), respectively. The position of TCC was determined using the methodology of Ref. 24. Single-beam mispointing errors with respect to TCC were of the order of 7 μm rms. This constrains the uncertainty of the location of true TCC. In addition, the measured uncertainty of the target position relative to TCC varied from shot to shot and was between 1.3 and 5.4 μm for all shots considered here. Two targets were shot at each position, one with D_2 fill and one with DT fill, with an additional D_2 shot at TCC to assess shot-to-shot repeatability.

III. SIMULATIONS AND COMPARISONS WITH EXPERIMENTAL DATA

The experiments were simulated with the 2D radiation–hydrodynamic code *DRACO*[25] using the first-principles equation of state (FPEOS).[29,30] *DRACO* is a 2D arbitrary Lagrangian–Eulerian (ALE) code for simulating direct-drive physics. It includes a full 3D ray trace model of laser absorption including a fully 3D CBET model described in Ref. 11. Laser energy deposition is then averaged azimuthally onto a 2D spherical axisymmetric grid. Thermal transport can be treated either locally with a variable flux-limited Spitzer model or a nonlocal model using a modified[31] Schurtz–Nicolaï–Busquet[32] (SNB) model. The flux limiter values used for all VFL simulations are shown in Table I are varied linearly between the times listed. It should be pointed out that while the nonlocal thermal transport model referred to in Ref. 17 used a Vlasov–Krook-type model,[33] this paper uses an SNB model. For simulations of OMEGA experiments, however, it has been shown that these models agree very well when the SNB thermal model is substituted for a flux-limited model with $f = 0.06$ during the first picket pulse,[34] which is the methodology used in this paper.

For each of the shots from Sec. II, four simulations were performed: (1) VFL with no target offset, (2) VFL with measured offset, (3) CBET with nonlocal thermal transport (CBET–NLTT) and no offset, and (4) CBET–NLTT with measured offset. In addition, for one D_2 shot (88575), additional offsets were simulated in 10-μm intervals to illustrate the yield degradation as a function of target offset for both CBET–NLTT and VFL models. The time-dependent flux-limiter values used in the VFL simulations were tuned to match both shock and shell trajectories obtained using the more detailed CBET–NLTT models, such that the in-flight adiabats and convergence ratios were the same. The only other nonuniformity imposed in these simulations was from the OMEGA beam geometry. While it is important to recognize that the neutron yield in experiments is predicted to be affected significantly by other nonuniformities, particularly laser imprint and capsule nonuniformities, relative trends in yields between targets omitting these other factors in simulation still provide a useful comparison of the yield degradation due to target offset. Furthermore, the target offsets were chosen to be large enough that the performance degradation due to low-mode asymmetry in the laser drive is expected to be dominated by the target offset.

TABLE I. Time history of the variable flux limiter values. Values are linearly interpolated between the times indicated.

Time (ns)	Flux-limiter value
0.0	0.085
0.3	0.085
1.0	0.08
1.8	0.06
2.3	0.045
2.4	0.045

The resolution in the simulations presented here was approximately 210 zones radially and 300 zones in theta from 0° to 180°. In our estimation, this is sufficient to resolve Legendre ℓ modes up to about 60 radially and 40 azimuthally. The criteria on which these estimates are based are (1) maintaining throughout the laser drive portion of the simulation a minimum of five zones radially across the extent of each half of the Rayleigh–Taylor (RT) instability[3] eigenmode (the half-width of which is estimated as the radial interval from the ablation front to a distance $1/k$ from the ablation front, where k is the mode wavenumber given by $k \equiv 2\pi/\lambda \simeq R_{abl}/\ell$, where R_{abl} is the average radius of the ablation front and varies as a function of time), (2) a minimum of 5 zones radially across the interval between the ablation front and a point radially outward from the ablation front at a distance equal to the density scale length during the same time interval, and (3) a minimum of 16 zones transversely across a single wavelength. Detailed convergence studies performed previously in *DRACO* indicate that when these criteria are satisfied, the acceleration-phase RT growth rates are generally accurate to within a few percent (see Ref. 35, p. 134). So, effectively, modes up to at least $\ell = 40$ are well resolved in these simulations, which is more than adequate to resolve the perturbation modes induced by the laser beam geometry and target offset. One single high-resolution simulation was also performed and used double the resolution, resolving modes up to $\ell = 80$.

Normalized fusion yields for both the experiments and simulations are plotted in Fig. 2. The experimentally measured offset magnitudes and directions, gas fill types, and absolute and normalized yields from each shot are shown for reference in Table II. In experiments, the

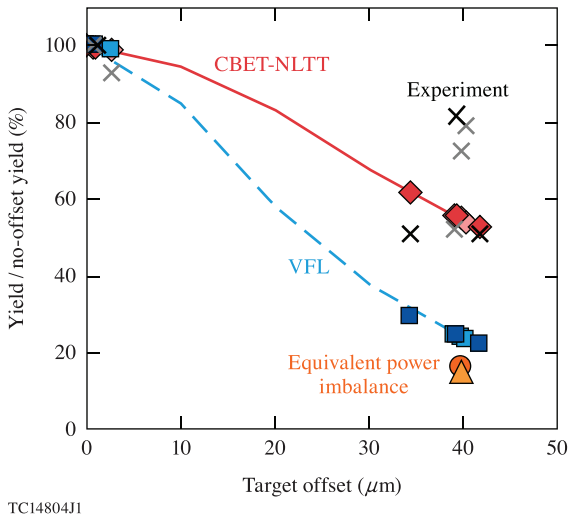

FIG. 2. Normalized neutron yields for *DRACO* simulations [CBET–NLTT (red diamonds); VFL (blue squares)] and experiments (×'s). Experiments are normalized to the nominal no-offset shot for each D_2 and DT series, whereas simulations of the same shots with as-measured target offsets are normalized to a no-offset case of the same shot. D_2 shots are shown in lighter colors. Normalized yields are shown for shot 88575 varying the target offset in simulations [CBET–NLTT (solid red line); VFL (dashed blue line)]. For comparison, two simulations with a power-imbalance–induced $\ell = 1$ asymmetry equivalent to that of a 40-μm target offset at $t = 0$ were modeled [CBET–NLTT (orange circle); VFL (light orange triangle)].

yields for each of the D_2 and DT shot sequences are normalized to their respective TCC reference shots, which were performed with (nominally) no offset. In simulation, the yield from each offset simulation is divided by the corresponding no-offset simulation of the same shot number. In Fig. 2, the lines plot *DRACO* simulations with varying offsets for shot 88575 with the CBET–NLTT model (solid red line) and the VFL model (dashed blue line). The simulations with the as-measured target offsets are shown by the red diamonds (CBET–NLTT) and blue squares (VFL). Experimental data are shown by the ×'s. Normalized yields are shown for both the D_2 shots (lighter colors) and DT shots (darker colors). The D_2 TCC shot (88572) with higher measured offset appears as the gray × at 2.6-μm offset (as-measured), and had a yield that was 93% of the other (offset 0.6 μm) D_2 TCC shot (88578). Actual yields (see Table II) varied from 2.8×10^{10} to 5.4×10^{10} for the D_2 shots and 1.3×10^{12} to 2.5×10^{12} for the DT shots. The measurement uncertainty in fusion yield is approximately 9% for the D_2 shots and 5% for the DT shots. The absolute ratio of experimental yields to simulated CBET–NLTT yields (with measured offsets) ranged from 16% to 28%. The single high-resolution 2D *DRACO* simulation including laser imprint modes up to $\ell = 80$ suggested that the discrepancy in absolute yields is due mostly to high-frequency modulations in the laser illumination being imprinted on the target.

It is noted that there is substantial variation in the yields for the offset implosions. Given that this variation is larger than the experimental uncertainty, it is hypothesized that this variation is due to directional interactions with the target-mounting stalk (similar to what was reported in Ref. 36) and other systematic and/or random variations between shots (e.g., laser power imbalance), which are also not modeled in these simulations. In these experiments, the stalk was located at the H2 port located at $(\theta, \phi) = (37.38°, 90.0°)$ and forms angles of 79.2°, 100.8°, and 54.3° with the P6, P7, and orthogonal offset directions, respectively. This assertion of directional interactions with the mounting stalk is difficult to corroborate, however, in the absence of a 3D simulation capability with a fully 3D CBET laser ray trace model, that is, relevant for direct-drive implosions.

A visual inspection of the simulation data in Fig. 2 reveals that the fusion yields drop significantly with increasing target offset when simulated with the VFL model without CBET. When simulated including CBET–NLTT physics, however, the degradation in yield due to offset is reduced substantially. This difference occurs even for small target offsets. To separate the effects of the CBET physics and NLTT physics on yield degradation, another set of simulations was performed with NLTT, but not CBET. The normalized yield trends from these simulations (not plotted here) closely matched the VFL trends, indicating that NLTT physics plays almost no role in mitigating the yield degradation from offset. This perhaps is not surprising, given that the multidimensional effects of NLTT physics are expected to manifest mainly in the mitigation of short-wavelength instability growth via a broadening of the density scale length at the ablation front and an increased ablation velocity.[3,37] Based on these simulation results, it can be concluded that CBET physics provides the mechanism that reduces the yield sensitivity to target offset. Furthermore, the simulated CBET–NLTT normalized yields match much more closely the observed experimental yields than the VFL data.

TABLE II. Experimental yields and target offsets from the OMEGA shots. The normalized yield ("yield over nominal TCC") is shown in the last column.

Shot number	Gas fill	Offset (μm)	Offset direction	Expt. yield	Yield over nominal TCC (%)
88572	D_2	2.6	Nominal TCC	$5.0 \times 10^{+10}$	93
88575	D_2	39.9	Toward P6	$3.9 \times 10^{+10}$	73
88576	D_2	40.3	Toward P7	$4.3 \times 10^{+10}$	79
88577	D_2	39.1	Orthogonal	$2.8 \times 10^{+10}$	53
88578	D_2	0.6	Nominal TCC	$5.4 \times 10^{+10}$	100
88579	DT	1.0	Nominal TCC	$2.5 \times 10^{+12}$	100
88581	DT	39.3	Toward P6	$2.1 \times 10^{+12}$	82
88583	DT	41.9	Toward P7	$1.3 \times 10^{+12}$	51
88584	DT	34.4	Orthogonal	$1.3 \times 10^{+12}$	51

On the D_2 shots, four x-ray framing cameras (XRFCs) collected time-resolved images of the coronal x-ray self-emission during the acceleration phase of the implosion from different views. These images were then used to infer the position of the ablation surface in 3D and calculate the position of the centroid of the coronal ring of x-ray emission in 3D space as a function of time using the methodology of Ref. 38. Using *SPECT3D*, a radiation transport post-processing code, corresponding time-resolved self-emission images were generated from the simulated *DRACO* data including the effects of experimental filters and instrument response functions. The images were generated along a diagnostic line of sight orthogonal to the target offset and analyzed to compare with the experimental images from the XRFC's. The results from both experiment and simulation show that the capsule centroid experiences a spatial drift away from its initial position that is approximately linear when plotted vs the distance traveled by the shell. When the capsule radius was compressed to approximately 150 μm, the distance traveled by the capsule center from its original position in the offset shots was measured experimentally to be between 9.2 to 10.0 μm along the offset direction with a 1.1- to 1.5-μm movement orthogonal to the offset direction (the measurement uncertainty was ± 1.0 μm). The orthogonal movement is attributed to nonuniformity sources other than the target offset. Reasonable agreement with experiment is seen in simulations with the CBET–NLTT model, which indicates the center drift along the offset direction at the same time is 12.0 μm. By contrast, the VFL model predicts a center drift of 16.6 μm, which is well outside the experimental error bars.

In addition to these time-resolved x-ray images, time-integrated self-emission x-ray images of the hot-spot core emission were obtained from the gated monochromatic x-ray imager (GMXI).[39] The centroid of the hot-spot x-ray emission was located following the methodology of Ref. 24 and compared with the DT TCC reference shot 88579 to calculate the distance between the centroids of the two imploded hot-spot cores. For reference, the measured initial offsets of these capsules from TCC were 0.6 (88579) and 39.3 μm (88581). Simulated time-integrated images of the core x-ray emission were likewise generated from *DRACO* using *SPECT3D* to compare with the GMXI images. The data from shot 88581 are shown in Fig. 3. The top images, (a) and (c) respectively, are the density contour of the target at peak compression from the VFL *DRACO* simulation and the corresponding time-integrated x-ray image from *SPECT3D* for shot 88581, whereas images (b) and (d) are the same, respectively, for the CBET–NLTT model. Image (e) is the experimental image from GMXIc. In each image, the position of TCC is shown by the white "×" symbol. The experimental distance between the centroid of x-ray emission of shots 88581 and the reference shot was measured as 61 ± 2 μm. Analysis of the simulated radiographs resulted in distances of 63 and 71 μm for the CBET–NLTT and VFL, respectively, showing that the best agreement between simulations and experiments is achieved when the CBET–NLTT model is used.

Although the purpose of generating these simulated GMXI images is mainly to compare the locations of the simulated and experimental hot-spot centroids in an offset shot relative to the TCC reference shot, the images also show similar size and shape of the hot spot. The average hot spot radius is approximately 44 μm in simulation and 48.5 μm in experiment. The difference between the two is likely due to the fact that the simulations, due to the finite computation resources available, did not model short wavelength perturbations caused by laser imprint and capsule surface imperfections, which can reduce overall capsule compressibility.

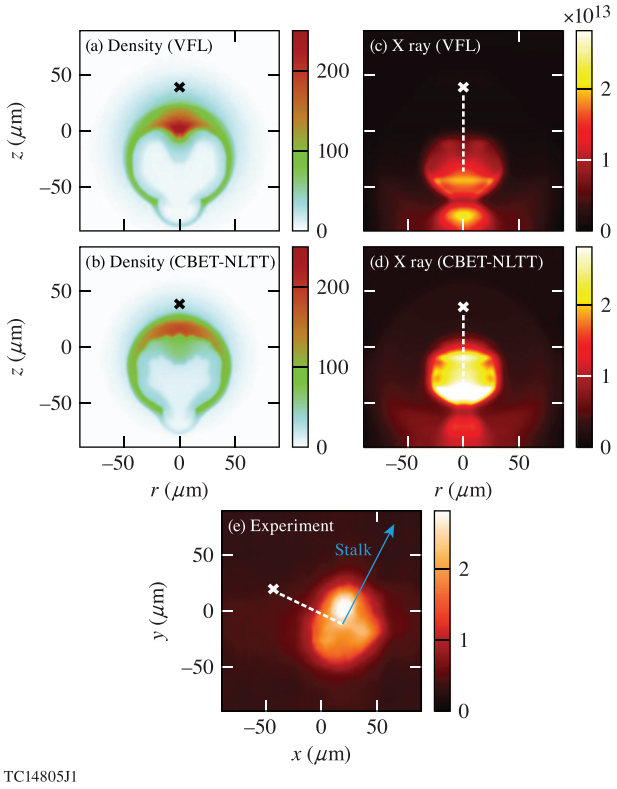

FIG. 3. Density plot (g/cm^3) at stagnation from *DRACO* simulations of shot 88581 with VFL (a) and CBET–NLTT (b). Simulated time-integrated x-ray images generated by *SPECT3D* from these simulations are shown in (c) VFL and (d) CBET–NLTT with arbitrary units. The experimental image from GMXIc is shown in (e). In all images, the location of TCC is shown by the × and the distance between TCC and centroid of emission is indicated by the white line. The position of the target mounting stalk is shown by the blue arrow in (e).

It should be noted that in the experimental image, the small bright spot near the top appears approximately at the angle where the target-mounting stalk is attached to the target [the stalk location was port H2, see the blue arrow in Fig. 3(e)], indicating that some stalk material may be present in the hot spot at that location. Since the stalk material is largely silicon, it is expected to emit much more brightly than the background hydrogenic and CH plasma when heated up to hot-spot temperatures of a few keV.

An attempt was made to distinguish between the CBET–NLTT and VFL models using both bulk hot-spot flow and T_{ion} asymmetry measurements using the methodology of Ref. 40. However, the differences between the two models was small enough to be within the experimental error bars.

IV. ANALYSIS

This mitigation of offset implosion nonuniformity by CBET physics can be understood largely as a geometrical effect. The initial displacement of the target away from TCC results in a perturbation in the laser illumination pattern that is dominated by an $\ell = 1$ mode,

where the "hot" side of the target is the one opposite the offset direction vector. As the corona forms, light rays from each beam will refract away from the edge of the target, eventually exiting the corona on a radially outbound trajectory. As the rays turn, they can interact with inbound rays from other beams, transferring light energy from one beam to another. In offset targets, the energy in these over-the-horizon rays is asymmetric about the capsule. Specifically, there is more over-the-horizon laser light refracting past the target on trajectories outbound toward the beams on the hot side. The increased outbound laser light on the hot side stimulates more CBET losses from the incoming beams on the hot side, as compared to the cold side, effectively reducing the $\ell = 1$ illumination nonuniformity.

To confirm the geometric nature of this CBET effect on target offset, both CBET–NLTT and VFL *DRACO* simulations were performed with zero offset, but instead with an induced $\ell = 1$ using a prescribed laser power imbalance. Specifically, the power-imbalance $\ell = 1$ intensity pattern on target was generated by multiplying the average, single-beam laser power by a function of the form $f(\theta_b) = 1 + AP_1[\cos(\theta_b)]$, where θ_b is the polar-angle coordinate of the each beam in the OMEGA target chamber, and $P_1[x] = x$ is the first-order ($\ell = 1$) Legendre polynomial. This results in an incident intensity profile matching very well a pure $\ell = 1$ Legendre mode, with some additional modes introduced by the discrete beam geometry (these modes are also present in the target offset simulations). The amplitude A of the modulating function was then chosen to match the $t = 0$ amplitude in laser intensity for the 40-μm offset. The resulting normalized yields, shown in Fig. 2 by the orange circle (CBET–NLTT) and light orange triangle (VFL), respectively, are very close to each other and similar to that of the VFL 40-μm offset simulation, indicating little mitigation of the power-imbalance–induced $\ell = 1$ by CBET. Specifically, the difference in normalized yield between VFL and CBET-NLTT was 15.2% to 16.4%, a difference of only 1.2% in absolute normalized yield or 7.9% relative increase in yield, compared to the offset case, where the difference in normalized yield was 24.1% to 54.5%, or a difference of 30.3% in absolute normalized yield or a 126% relative yield increase. Since the power-imbalance and target offset cases start with the same $\ell = 1$ amplitude in the laser intensity, it appears that the difference in laser intensity from the hot side to the cold side accounts for only a very small portion of the $\ell = 1$ mitigation by CBET in these simulations, whereas the much larger effect is geometric in the case of target offset.

Because target offset can also be considered as a coherent mispointing or repointing of all the laser beams in a single direction away from the center of the target, it is possible that a similar $\ell = 1$ and/or higher-mode mitigation effect occurs when laser beams are imprecisely pointed, as happens in all laser systems to varying extents. However, since imprecise beam pointing generally results in a random statistical mispointing of the beams in 3D, rather than a coherent, single-direction mispointing of all beams, the effect of CBET on mispointing symmetry is likely to be smaller than for target offset. It should be pointed out that the illumination pattern due to random beam mispointing typically has a broader spectrum than that due to the target offset.[41] For example, this spectrum usually contains $\ell = 2$ and $\ell = 3$ modes with $m = 0$ and $m \neq 0$ components often being present at amplitudes of the order of 30% to 50% of the $\ell = 1$ mode. Because of this, there is no clear axis of symmetry that can be readily exploited in a 2D axisymmetric hydrodynamics code such as *DRACO*. Therefore, quantifying any mitigating effect of CBET on implosions asymmetry due to beam mispointing using *DRACO* is not ideal and not attempted in this paper.

An effect similar to this is also observed in simulations and experiments of polar-drive[42] experiments[11] that show CBET is higher at the equator where beams are pointed away from the target center to improve illumination uniformity. It is also related to experiments where the beam-to-target size ratio is reduced[43,44] to mitigate CBET.

DRACO's in-line scattered-light diagnostic confirms that there is more laser light scattered due to CBET from the hot side of the target than from the cold side. Figure 4 shows a snapshot at the time of peak laser power ($t = 2.1$ ns) of the intensity of the simulated scattered light (Hammer projection) that is collected at different angular positions of the inner surface of the target chamber for (a) the VFL model and (b) the CBET–NLTT model. First, it should be noted that the VFL model without CBET showed higher refracted light intensity on the hot side (north pole, i.e., $\theta = 0°$) opposite to the direction of the offset ($\theta_{\text{offset}} = 180°$), than on the "cold side" (south pole, i.e., $\theta = 180°$), as explained earlier. Furthermore, with the CBET–NLTT model, the simulation showed enhanced scattered light at the hot-side. Specifically, the scattered light at the north pole increased with the addition of CBET by approximately twofold relative to the VFL simulation, whereas the scattered light at the cold south pole increased by only about 20%.

Figure 5 plots the time history of the $\ell = 1$ asymmetry in the laser drive. At 50-ps intervals, the laser energy deposited in the plasma was radially summed, divided by the original target surface area to obtain an effective on-target laser intensity, and then the spherical

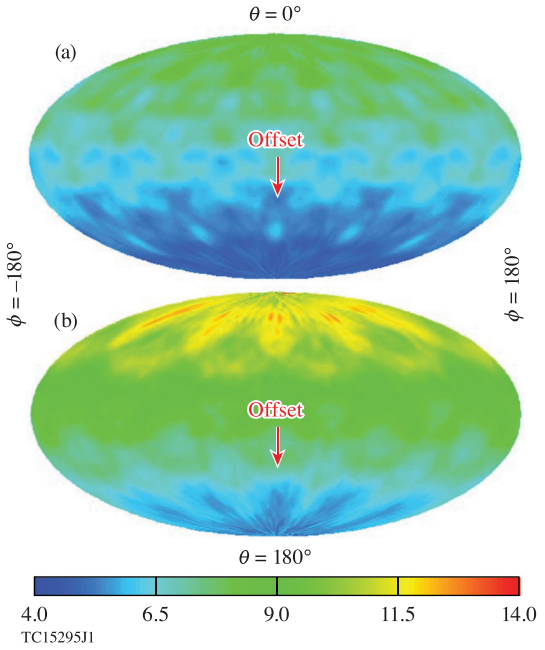

FIG. 4. Hammer projection plot of the simulated scattered light at the OMEGA target chamber radius (10^6 W/cm^2) at the time of peak laser intensity using (a) the variable flux limiter model and (b) CBET plus nonlocal thermal transport. Both simulations have a 40-μm target offset in the direction $\theta = 180°$.

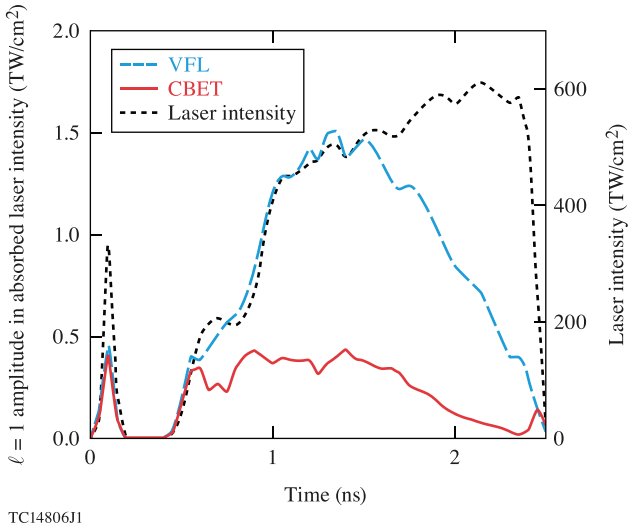

FIG. 5. The time evolution of the $\ell = 1$ amplitude (absolute value) in the absorbed laser intensity is plotted vs time for both the CBET–NLTT (solid red line) and VFL (dashed blue line). The laser pulse is plotted (dotted gray line) for reference.

harmonic mode $\ell = 1$ ($m = 0$) was extracted. Results from both the CBET–NLTT (solid line) and VFL (dashed line) *DRACO* simulations of shot 88575 using the as-measured offset were plotted. During the initial picket pulse, both models show similar $\ell = 1$ amplitudes, but as the corona develops a longer density scale length and the laser intensity is increased, the two models deviate substantially as CBET scattering amplifies. By the beginning of the rise from the foot to the main drive, at about 0.9 ns, the VFL mode shows the $\ell = 1$ mode rising proportional to the laser power, whereas the CBET $\ell = 1$ plateaus. At this time, the density scale length, $L_\rho \equiv \rho(\partial\rho/\partial r)^{-1}$, and velocity scale length, $L_v \equiv v(\partial v/\partial r)^{-1}$, at the quarter critical density are approximately 100 and 180 μm, respectively. The electron and ion temperatures are $T_e = 1.5$ keV and $T_i = 0.7$ keV. At 1.5 ns, the $\ell = 1$ amplitude for both models decreases approximately linearly in time, due both to a decrease of the critical surface radius as the target implodes and to refractive effects, both of which increase the effective ratio of laser beam spot to target radius. By the end of the pulse at 2.3 ns, the scale lengths have increased to $L_\rho = 180$ μm and $L_v = 340$ μm, and the temperatures to $T_e = 2.3$ keV and $T_i = 1.1$ keV. As the pulse ends and the laser power is ramped down, the incident laser intensity decreases, CBET effectively turns off, and the $\ell = 1$ mode in the CBET simulation increases until it matches the VFL model, as expected in the absence of CBET. Overall, it is clear from Fig. 5 that the $\ell = 1$ mode is driven more strongly without CBET than with CBET.

It should be noted that the results presented in Ref. 12 using the code *ASTER* showed that for an offset target, the normalized yield *decreased* and the displacement of the target centroid at peak compression *increased* when modeled with CBET and Spitzer heat transport compared to a VFL, no-CBET calculation. Those results were interpreted to suggest that flux-limited heat flow can underestimate the effect of laser-imposed nonuniformities because of a higher coronal temperature, which results in larger lateral heat smoothing. The results in this paper, however, indicate that (1) an NLTT heat flow model gives very similar results to the VFL model with respect to the $\ell = 1$ nonuniformity; and (2) that the $\ell = 1$ yield degradation is largely unaffected by the difference in coronal temperature. Note also that the CBET model[45] in those *ASTER* simulations used a reduced-dimensional model that is not expected to capture the multidimensional effect of CBET from multiple beams on illumination nonuniformities. This reduced model assumed 1D spherically-symmetric coronal profiles and did not track rays through the full 3D space, but rather traced rays in 2D. Furthermore, *ASTER* only tracked the radial position of rays, such that rays at different (θ, ϕ) coordinates, but same radial coordinate, were allowed to interact and exchange energy even though they were physically located at different points in space. Direction vectors of rays for computing CBET were only two-dimensional. Finally, the effects of target offset and beam mispointing were calculated in a simplified manner. The laser deposition profile was computed with the beam aimed at the target center, then the deposition profile was shifted perpendicular to the beam axis according to the direction and magnitude of the target offset and/or mispointing. An accounting was also made for the change in orientation of the normal vector to the target surface at all points.

In contrast, the CBET laser physics package[11] in *DRACO* captures the interactions of beams with each other and the background plasma by performing a full ray trace in 3D, modeling the positions and angles of each beam for any arbitrary chosen beam geometry, including the correct positioning of the target relative to the center of beam convergence. Cylindrical symmetry in 2D is assumed only in the plasma conditions. The OMEGA illumination pattern on the surface of an offset target retains approximately 2D axisymmetry about the vector between the capsule center and TCC. Deviation from 2D axisymmetry is largely contained in the $\ell = 10$, $m = 5$ mode, which is more than five times lower in amplitude than the $\ell = 1$ mode induced by a target offset of 5 μm under the beam and target conditions of these experiments. This approximate axisymmetry has been shown in previous 3D simulations[41] using the code *HYDRA*,[46] where the amplitude of the $\ell = 1$ perturbation and total rms illumination nonuniformity were virtually unchanged when the offset vector was rotated relative to the laser system. Therefore, a 2D axisymmetric treatment of the hydrodynamics with a 3D raytracing model of laser energy deposition including CBET is sufficient to capture the essential $\ell = 1$ physics of target offset when the target offset vector is aligned with the axis of symmetry.

V. CONCLUSIONS

In conclusion, cross-beam energy transfer in direct-drive inertial confinement fusion has been shown in simulation to mitigate the $\ell = 1$ implosion asymmetry caused by a target offset. Over-the-horizon scattered light is increased on the hot-side (higher intensity, opposite the target offset vector) of the target inducing increased CBET losses on the hot side, providing a negative feedback mechanism for reducing absorption on the hot side. This is a similar effect to what has been observed previously in simulations and experiments with either smaller laser spots or in a polar direct-drive beam geometry.

Simulations modeling a target offset require a 3D laser ray-trace model with CBET physics to accurately capture the implosion asymmetry and yield degradation. When 3D CBET physics was included in the laser ray-trace model, simulated observables better reproduced experimental data for the three complementary observables described

here: neutron yield, early-time drift of the target centroid, and the position of the x-ray time-integrated hot-spot centroid.

Although CBET is shown to mitigate the asymmetry due to a target offset, proposed CBET mitigation techniques may reduce this effect, resulting in enhanced sensitivity to target offset than what is currently seen in experiments. While such CBET mitigation is expected to improve overall implosion performance, the use of such strategies will likely require more stringent target offset tolerances than those which are currently considered acceptable and are derived from direct-drive experiments where no CBET mitigation techniques were used. The effect of CBET-mitigation techniques on implosion degradation due to a target offset will be discussed in an upcoming publication.

ACKNOWLEDGMENTS

The authors thank I. E. Golovkin of PrismSPECT for his help with optimizing the post-processing code *SPECT3D*.

This material is based upon work supported by the Department of Energy National Nuclear Security Administration under Award No. DE-NA0003856, the University of Rochester, and the New York State Energy Research and Development Authority.

DATA AVAILABILITY

The data that support the findings of this study are available from the corresponding author upon reasonable request.

REFERENCES

[1]R. S. Craxton, K. S. Anderson, T. R. Boehly, V. N. Goncharov, D. R. Harding, J. P. Knauer, R. L. McCrory, P. W. McKenty, D. D. Meyerhofer, J. F. Myatt, A. J. Schmitt, J. D. Sethian, R. W. Short, S. Skupsky, W. Theobald, W. L. Kruer, K. Tanaka, R. Betti, T. J. B. Collins, J. A. Delettrez, S. X. Hu, J. A. Marozas, A. V. Maximov, D. T. Michel, P. B. Radha, S. P. Regan, T. C. Sangster, W. Seka, A. A. Solodov, J. M. Soures, C. Stoeckl, and J. D. Zuegel, Phys. Plasmas **22**, 110501 (2015).

[2]J. Nuckolls, L. Wood, A. Thiessen, and G. Zimmerman, Nature **239**, 139 (1972).

[3]Lord Rayleigh, in *Scientific Papers* (Cambridge University Press, Cambridge, England, 1900), Vol. II, p. 200; G. Taylor, Proc. R. Soc. London, Ser. A **201**, 192 (1950); H. Takabe, K. Mima, L. Montierth, and R. L. Morse, Phys. Fluids **28**, 3676 (1985); R. Betti, V. N. Goncharov, R. L. McCrory, and C. P. Verdon, Phys. Plasmas **5**, 1446 (1998).

[4]R. D. Richtmyer, Commun. Pure Appl. Math. **13**, 297 (1960); A. L. Velikovich, J. P. Dahlburg, J. H. Gardner, and R. J. Taylor, Phys. Plasmas **5**, 1491 (1998); V. N. Goncharov, Phys. Rev. Lett. **82**, 2091 (1999).

[5]G. I. Bell, Report No. LA-1321 (Los Alamos National Laboratory, Los Alamos, NM, 1951); M. S. Plesset, J. Appl. Phys. **25**, 96 (1954); R. Epstein, Phys. Plasmas **11**, 5114 (2004).

[6]C. J. Randall, J. R. Albritton, and J. J. Thomson, Phys. Fluids **24**, 1474 (1981).

[7]C. J. McKinstrie, J. S. Li, R. E. Giacone, and H. X. Vu, Phys. Plasmas **3**, 2686 (1996).

[8]C. J. McKinstrie, A. V. Kanaev, V. T. Tikhonchuk, R. E. Giacone, and H. X. Vu, Phys. Plasmas **5**, 1142 (1998).

[9]I. V. Igumenshchev, D. H. Edgell, V. N. Goncharov, J. A. Delettrez, A. V. Maximov, J. F. Myatt, W. Seka, A. Shvydky, S. Skupsky, and C. Stoeckl, Phys. Plasmas **17**, 122708 (2010).

[10]P. B. Radha, V. N. Goncharov, M. Hohenberger, T. C. Sangster, R. Betti, R. S. Craxton, D. H. Edgell, R. Epstein, D. H. Froula, J. A. Marozas, F. J. Marshall, R. L. McCrory, P. W. McKenty, D. D. Meyerhofer, D. T. Michel, S. X. Hu, W. Seka, A. Shvydky, S. Skupsky, J. A. Frenje, M. Gatu Johnson, R. D. Petrasso, T. Ma, S. Le Pape, and A. J. Mackinnon, J. Phys.: Conf. Ser. **688**, 012006 (2016).

[11]J. A. Marozas, M. Hohenberger, M. J. Rosenberg, D. Turnbull, T. J. B. Collins, P. B. Radha, P. W. McKenty, J. D. Zuegel, F. J. Marshall, S. P. Regan, T. C. Sangster, W. Seka, E. M. Campbell, V. N. Goncharov, M. W. Bowers, J.-M. G. Di Nicola, G. Erbert, B. J. MacGowan, L. J. Pelz, and S. T. Yang, Phys. Rev. Lett. **120**, 085001 (2018).

[12]I. V. Igumenshchev, V. N. Goncharov, F. J. Marshall, J. P. Knauer, E. M. Campbell, C. J. Forrest, D. H. Froula, V. Yu Glebov, R. L. McCrory, S. P. Regan, T. C. Sangster, S. Skupsky, and C. Stoeckl, Phys. Plasmas **23**, 052702 (2016).

[13]S. X. Hu, D. T. Michel, A. K. Davis, R. Betti, P. B. Radha, E. M. Campbell, D. H. Froula, and C. Stoeckl, Phys. Plasmas **23**, 102701 (2016).

[14]R. C. Malone, R. L. McCrory, and R. L. Morse, Phys. Rev. Lett. **34**, 721 (1975).

[15]L. Spitzer, Jr. and R. Härm, Phys. Rev. **89**, 977 (1953).

[16]J. Delettrez, Can. J. Phys. **64**, 932 (1986).

[17]I. V. Igumenshchev, V. N. Goncharov, W. T. Shmayda, D. R. Harding, T. C. Sangster, and D. D. Meyerhofer, Phys. Plasmas **20**, 082703 (2013).

[18]K. S. Anderson, P. W. McKenty, A. Shvydky, J. P. Knauer, T. J. B. Collins, and M. M. Marinak, in *58th Annual Meeting of the APS Division of Plasma Physics, San Jose, California, 31 October–4 November 2016* (American Physical Society, 2016), Vol. 61, no. 18, available at http://meetings.aps.org/link/BAPS.2016.DPP.NO5.11.

[19]P. W. McKenty, T. C. Sangster, M. Alexander, R. Betti, R. S. Craxton, J. A. Delettrez, L. Elasky, R. Epstein, A. Frank, V. Yu. Glebov, V. N. Goncharov, D. R. Harding, S. Jin, J. P. Knauer, R. L. Keck, S. J. Loucks, L. D. Lund, R. L. McCrory, F. J. Marshall, D. D. Meyerhofer, S. P. Regan, P. B. Radha, S. Roberts, W. Seka, S. Skupsky, V. A. Smalyuk, J. M. Soures, K. A. Thorp, M. Wozniak, J. A. Frenje, C. K. Li, R. D. Petrasso, F. H. S'eguin, K. A. Fletcher, S. Padalino, C. Freeman, N. Izumi, J. A. Koch, R. A. Lerche, M. J. Moran, T. W. Phillips, G. J. Schmid, and C. Sorce, Phys. Plasmas **11**, 2790 (2004).

[20]S. X. Hu, P. B. Radha, J. A. Marozas, R. Betti, T. J. B. Collins, R. S. Craxton, J. A. Delettrez, D. H. Edgell, R. Epstein, V. N. Goncharov, I. V. Igumenshchev, F. J. Marshall, R. L. McCrory, D. D. Meyerhofer, S. P. Regan, T. C. Sangster, S. Skupsky, V. A. Smalyuk, Y. Elbaz, and D. Shvarts, Phys. Plasmas **16**, 112706 (2009).

[21]T. J. B. Collins, J. A. Marozas, K. S. Anderson, R. Betti, R. S. Craxton, J. A. Delettrez, V. N. Goncharov, D. R. Harding, F. J. Marshall, R. L. McCrory, D. D. Meyerhofer, P. W. McKenty, P. B. Radha, A. Shvydky, S. Skupsky, and J. D. Zuegel, Phys. Plasmas **19**, 056308 (2012).

[22]T. R. Boehly, D. L. Brown, R. S. Craxton, R. L. Keck, J. P. Knauer, J. H. Kelly, T. J. Kessler, S. A. Kumpan, S. J. Loucks, S. A. Letzring, F. J. Marshall, R. L. McCrory, S. F. B. Morse, W. Seka, J. M. Soures, and C. P. Verdon, Opt. Commun. **133**, 495 (1997).

[23]S. Atzeni, A. Schiavi, L. Antonelli, and A. Serpi, Eur. Phys. J. D **73**, 243 (2019).

[24]W. Grimble, F. J. Marshall, and E. Lambrides, Phys. Plasmas **25**, 072702 (2018).

[25]P. B. Radha, V. N. Goncharov, T. J. B. Collins, J. A. Delettrez, Y. Elbaz, V. Yu. Glebov, R. L. Keck, D. E. Keller, J. P. Knauer, J. A. Marozas, F. J. Marshall, P. W. McKenty, D. D. Meyerhofer, S. P. Regan, T. C. Sangster, D. Shvarts, S. Skupsky, Y. Srebro, R. P. J. Town, and C. Stoeckl, Phys. Plasmas **12**, 032702 (2005).

[26]J. J. MacFarlane, I. E. Golovkin, P. Wang, P. R. Woodruff, and N. A. Pereyra, High Energy Density Phys. **3**, 181 (2007).

[27]V. N. Goncharov, J. P. Knauer, P. W. McKenty, P. B. Radha, T. C. Sangster, S. Skupsky, R. Betti, R. L. McCrory, and D. D. Meyerhofer, Phys. Plasmas **10**, 1906 (2003).

[28]K. Anderson and R. Betti, Phys. Plasmas Lett. **11**, 5 (2004).
[29]S. X. Hu, L. A. Collins, V. N. Goncharov, T. R. Boehly, R. Epstein, R. L. McCrory, and S. Skupsky, Phys. Rev. E **90**, 033111 (2014).
[30]S. X. Hu, L. A. Collins, V. N. Goncharov, J. D. Kress, R. L. McCrory, and S. Skupsky, Phys. Rev. E **92**, 043104 (2015).
[31]D. Cao, G. Moses, and J. Delettrez, Phys. Plasmas **22**, 082308 (2015).
[32]G. P. Schurtz, Ph. D. Nicolaï, and M. Busquet, Phys. Plasmas **7**, 4238 (2000).
[33]V. N. Goncharov, T. C. Sangster, P. B. Radha, R. Betti, T. R. Boehly, T. J. B. Collins, R. S. Craxton, J. A. Delettrez, R. Epstein, V. Yu. Glebov, S. X. Hu, I. V. Igumenshchev, J. P. Knauer, S. J. Loucks, J. A. Marozas, F. J. Marshall, R. L. McCrory, P. W. McKenty, D. D. Meyerhofer, S. P. Regan, W. Seka, S. Skupsky, V. A. Smalyuk, J. M. Soures, C. Stoeckl, D. Shvarts, J. A. Frenje, R. D. Petrasso, C. K. Li, F. Seguin, W. Manheimer, and D. G. Colombant, Phys. Plasmas **15**, 056310 (2008).
[34]D. Cao, Ph.D. thesis, University of Wisconsin–Madison, 2014.
[35]K. S. Anderson, Ph.D. thesis, University of Rochester, 2006.
[36]M. Gatu Johnson, P. J. Adrian, K. S. Anderson, B. D. Appelbe, J. P. Chittenden, A. J. Crilly, D. Edgell, C. J. Forrest, J. A. Frenje, V. Yu. Glebov, B. M. Haines, I. Igumenshchev, D. Jacobs-Perkins, R. Janezic, N. V. Kabadi, J. P. Knauer, B. Lahmann, O. M. Mannion, F. J. Marshall, T. Michel, F. H. Séguin, R. Shah, C. Stoeckl, C. A. Walsh, and R. D. Petrasso, Phys. Plasmas **27**, 032704 (2020).
[37]S. X. Hu, V. A. Smalyuk, V. N. Goncharov, S. Skupsky, T. C. Sangster, D. D. Meyerhofer, and D. Shvarts, Phys. Rev. Lett. **101**, 055002 (2008).
[38]D. T. Michel, I. V. Igumenshchev, A. K. Davis, D. H. Edgell, D. H. Froula, D. W. Jacobs-Perkins, V. N. Goncharov, S. P. Regan, A. Shvydky, and E. M. Campbell, Phys. Rev. Lett. **120**, 125001 (2018).
[39]F. J. Marshall and J. A. Oertel, Rev. Sci. Instrum. **68**, 735 (1997).
[40]O. M. Mannion, J. P. Knauer, V. Yu. Glebov, C. J. Forrest, A. Liu, Z. L. Mohamed, M. H. Romanofsky, T. C. Sangster, C. Stoeckl, and S. P. Regan, Nucl. Instrum. Methods Phys. Res., Sect. A **964**, 163774 (2020).
[41]K. S. Anderson, P. W. McKenty, A. Shvydky, T. J. B. Collins, C. J. Forrest, J. P. Knauer, F. J. Marshall, P. B. Radha, A. B. Sefkow, and M. M. Marinak, Bull. Am. Phys. Soc. **62**, BAPS.2017.DPP.UO7.3 (2017).
[42]S. Skupsky, J. A. Marozas, R. S. Craxton, R. Betti, T. J. B. Collins, J. A. Delettrez, V. N. Goncharov, P. W. McKenty, P. B. Radha, T. R. Boehly, J. P. Knauer, F. J. Marshall, D. R. Harding, J. D. Kilkenny, D. D. Meyerhofer, T. C. Sangster, and R. L. McCrory, Phys. Plasmas **11**, 2763 (2004).
[43]D. H. Froula, I. V. Igumenshchev, D. T. Michel, D. H. Edgell, R. Follett, V. Yu. Glebov, V. N. Goncharov, J. Kwiatkowski, F. J. Marshall, P. B. Radha, W. Seka, C. Sorce, S. Stagnitto, C. Stoeckl, and T. C. Sangster, Phys. Rev. Lett. **108**, 125003 (2012).
[44]I. V. Igumenshchev, W. Seka, D. H. Edgell, D. T. Michel, D. H. Froula, V. N. Goncharov, R. S. Craxton, L. Divol, R. Epstein, R. Follett, J. H. Kelly, T. Z. Kosc, A. V. Maximov, D. D. Meyerhofer, P. Michel, J. F. Myatt, T. C. Sangster, A. Shvydky, S. Skupsky, and C. Stoeckl, Phys. Plasmas **19**, 056314 (2012).
[45]I. V. Igumenshchev, personal communication (2018).
[46]M. M. Marinak, G. D. Kerbel, N. A. Gentile, O. Jones, D. Munro, S. Pollaine, T. R. Dittrich, and S. W. Haan, Phys. Plasmas **8**, 2275 (2001).